Investigation of Liquid Flow in Microchannels

Dong Liu* and Suresh V. Garimella[†]
Purdue University, West Lafayette, Indiana 47907-2088

Liquid flow in microchannels is investigated both experimentally and numerically. The experiments are carried out in microchannels with hydraulic diameters from 244 to 974 μm at Reynolds numbers ranging from 230 to 6500. The pressure drop in these microchannels is measured in situ and is also determined by correcting global measurements for inlet and exit losses. Onset of turbulence is verified by flow visualization. The experimental measurements of pressure drop are compared to numerical predictions. Results show that conventional theory may be used to predict successfully the flow behavior in microchannels in the range of dimensions considered here.

Nomenclature

D_h	=	hydraulic diameter, μm
f	=	Darcy friction factor
H	=	microchannel height, μm
L	=	microchannel length, mm
l	=	characteristic size of eddies in turbulent flow, m
P	=	pressure, Pa
Q	=	volume flow rate, m^3/s
Re	=	Reynolds number
U	=	average velocity in microchannel, m/s
u	=	characteristic velocity scale of eddies in turbulent flow, m/s
W	=	microchannel width, μm
x^+	=	entrance length, mm
α	=	aspect ratio, H/W
ΔP	=	pressure difference, Pa
δ	=	uncertainty
ε	=	dissipation rate, m^2/s^3
η	=	Kolmogorov length scale, m
μ	=	fluid viscosity, N $\cdot$ s/m^2
ν	=	kinematic viscosity, m^2/s
ρ	=	fluid density, kg/m^3
app	=	apparent
fd	=	fully developed conditions

Introduction

A NUMBER of investigations have been undertaken in the recent past to understand the fundamentals of fluid flow in microchannels, as well as to compare the heat transfer characteristics to those in conventional channels. This work has been driven in large part by the very high heat transfer rates that can be achieved with microchannel heat sinks for electronics cooling and other applications. However, published results have often been inconsistent, with wide discrepancies between different studies. For example, the friction factors have either been higher or lower than values predicted by classical laminar theory for conventional-sized (macro) channels.[1,2] Another discrepancy concerns early transition from laminar to turbulent flow.[1,3] Possible reasons advanced to account for the deviation from classical theory include surface roughness effects,[3]

*Graduate Research Assistant, Cooling Technologies Research Center, School of Mechanical Engineering. Student Member AIAA.
†Professor and Director, Cooling Technologies Research Center, School of Mechanical Engineering; sureshg@ecn.purdue.edu.

electrical double-layer effects,[4] and aspect ratio effects.[‡] The capability of Navier–Stokes equations to represent adequately the flow and heat transfer behavior in microchannels has been called into question by these studies.

Recent reviews of the state of the art[5,6] indicate that before predictions of flow and heat transfer rates in microchannels can be made with confidence, carefully designed experiments are needed to resolve the discrepancies in the literature and to provide practical information on the design of microchannel heat sinks.

In the present work, an experimental facility has been designed and fabricated to enable a careful investigation of single-phase liquid flow in microchannels with hydraulic diameters ranging from approximately 250 to 1000 μm. The Reynolds number of the flow was varied from 2.3×10^2 to 6.5×10^3. The aims of this work are first to examine the validity of conventional theory in predicting the flow behavior in microchannels and then to verify the Reynolds number range for transition from laminar to turbulent flow.

Experimental Apparatus

The experimental facility used for these experiments is shown schematically in Fig. 1. The facility consists of a liquid reservoir pressured by gas, microfilter, flowmeter, differential pressure transducer (diaphragm type) with carrier demodulator, microchannel test section, and computerized data acquisition system. A wide range of flow rates of deionized water from 0.08 to 1.06 l/min can be achieved by varying the gas pressure. A turbine flowmeter with an infrared flow sensor is used for measurement of flow rate. Optical access for flow visualization is available because the test section is made of plexiglass.

In the initial design, a variable-flow gear pump was used as the prime mover, but oscillations in the flow rate were observed. Because external perturbations could cause instability in the flow and interfere with flow transition, the test apparatus was revised for the flow to be driven by pressurized nitrogen gas. This approach was found to provide a smooth and steady flow, with pressures of up to 827 kPa (120 psi). When the pressure drop along the microchannel and the flow rate through the microchannel are measured, a friction factor is calculated.

Microchannel pressure measurements in the literature have been generally made between the inlet and exit of the test sections, beyond the actual length of the microchannels. Consequently, the measured pressure drops have inevitably included local losses due to the abrupt contraction at the inlet and the expansion at the outlet. It is crucial to account for these pressure losses appropriately to obtain sound results; however, the approach used for this correction has not been clarified in sufficient detail in many published studies. To address this question further, two types of microchannel test sections were

fabricated for the present work as described in the following, to determine the methodology needed to achieve reliable pressure drop results.

A schematic representing the two different types of microchannel test sections is shown in Fig. 2. The microchannel test sections were fabricated from plexiglass, using a three-axis Computer Numerically Controlled (CNC) machine. The desired microchannel widths and aspect ratios were achieved by selecting high-speed steel jeweler's saws of different thickness and controlling the cutting depth. A list of the microchannel test sections investigated is provided in Table 1. The resulting surface roughness within the microchannels was measured with a profilometer and found to yield relative roughness (defined as the ratio of measured absolute roughness to the characteristic length, that is, hydraulic diameter in the present study) of well below 3%. The effects of surface roughness are, thus, not likely to be critical in influencing the flowfield.[7] The dimensions of the microchannel cross section were also carefully measured with an optical microscope, minimizing the uncertainty in determining hydraulic diameters D_h.

The two types of microchannel test sections studied differ in two respects: the microchannel length and the position of pressure tap ports. For the first type, in which the microchannels are shorter (S series), the pressure taps were placed in the inlet and outlet sections, as shown by the dashed lines in Fig. 2. For the second type, the channel length is longer (L series), and the pressure taps were machined along the length of the microchannel itself, remote from the effects of the entrance and exit regions. A 100 μm-diam-microdrill was used for making the pressure taps. In this latter case, the measured pressure difference would be the actual pressure drop between the locations of the two pressure taps, with no additional considerations needed for losses. The pressure taps were carefully machined to avoid burs or other disturbances to the flow channel.

Data Reduction and Uncertainty Analysis

The experimental data in the present work were analyzed in the framework of conventional theory. The pressure drop and flow rate were measured to obtain the two most often used nondimensional parameters, the Reynolds number Re and the Darcy friction factor f:

$$Re = \rho U D_h / \mu \tag{1}$$

$$f = (\Delta P / L) D_h \big/ \left(\tfrac{1}{2}\right) \rho U^2 \tag{2}$$

The experimental measurements were compared to predictions from conventional theory. For fully developed laminar flow in rectangular channels of channel aspect ratio α, the following expression from the literature[8] was used to predict the friction constant:

$$f Re = 96(1 - 1.3553/\alpha + 1.9467/\alpha^2 - 1.7012/\alpha^3$$
$$+ 0.9564/\alpha^4 - 0.2537/\alpha^5) \tag{3}$$

For fully developed turbulent flow, predictions were obtained following the Blasius solution,

$$f = 0.316/Re^{0.25} \qquad (Re < 2 \times 10^4) \tag{4}$$

In most practical applications, the microchannel is not long enough for the flow to become fully developed under laminar flow conditions. In such cases, the following expression for apparent friction factor accounts for both the developing and fully developed laminar flow regions in the channel[8]:

$$f_{\text{app}} Re = \left[\{3.2/(x^+)^{0.57}\}^2 + (f Re)_{\text{fd}}^2 \right]^{\frac{1}{2}} \tag{5}$$

where $(f Re)_{\text{fd}}$ is calculated as in Eq. (3) and the entrance length x^+ is defined as

$$x^+ = L/(D_h \cdot Re)$$

Similarly well-established correlations are, however, unavailable for turbulent developing flows.

Modifications must be made when calculating pressure drops for the short microchannels to exclude the pressure losses resulting from the inlet contraction and outlet expansion. The correction methodology used in this work is discussed in the Appendix. The pressure

Table 1 Dimensions of the microchannels tested

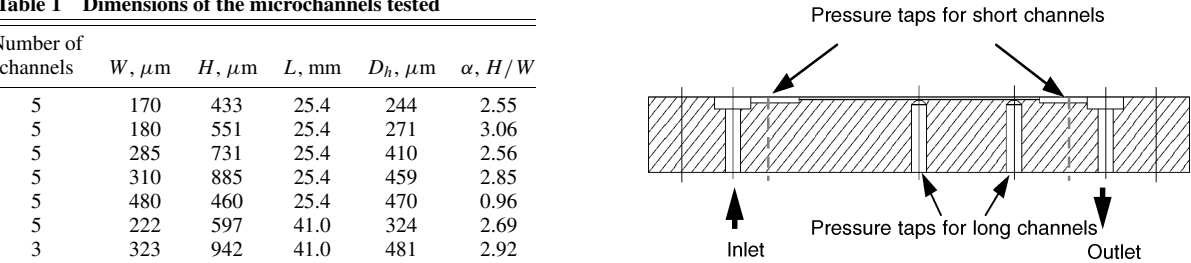| Test number	Number of channels	W, μm	H, μm	L, mm	D_h, μm	$\alpha, H/W$
S1	5	170	433	25.4	244	2.55
S2	5	180	551	25.4	271	3.06
S3	5	285	731	25.4	410	2.56
S4	5	310	885	25.4	459	2.85
S5	5	480	460	25.4	470	0.96
L1	5	222	597	41.0	324	2.69
L2	3	323	942	41.0	481	2.92
L3	3	450	384	41.0	414	0.85
L4	3	1061	900	41.0	974	0.85

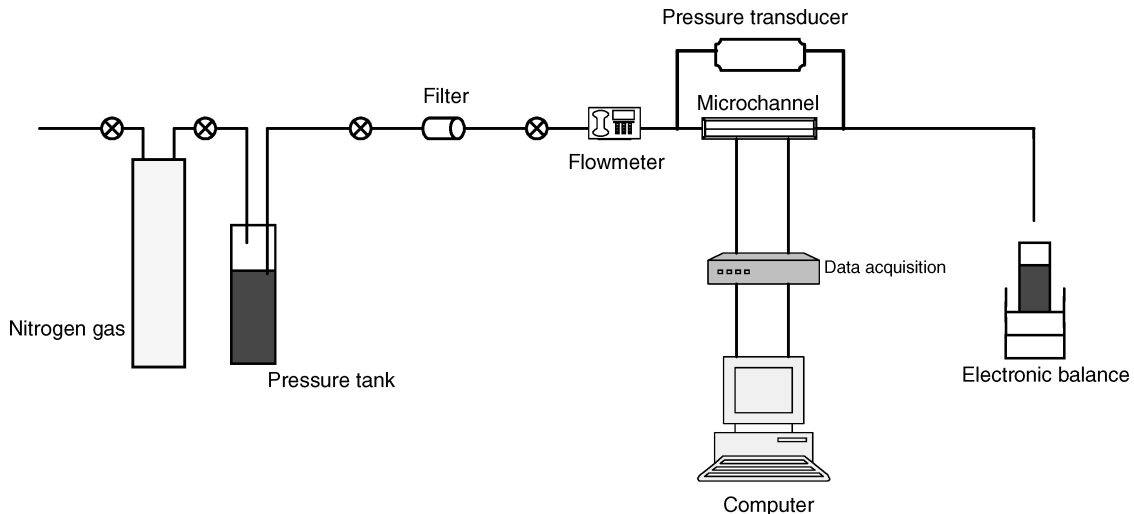Fig. 2 Schematic of the microchannel test section (top cover not shown).

Fig. 1 Schematic of the experimental apparatus.

drop to be used in Eq. (2) for the short microchannels is then

$$\Delta P = (\Delta P)_{\text{measured}} - (\Delta P)_{\text{loss}} \qquad (6)$$

The experimental uncertainties in the measurements were estimated using[9]:

$$\frac{\delta Re}{Re} = \left[\left(\frac{\delta Q}{Q}\right)^2 + \left(\frac{\delta H}{H}\right)^2 + \left(\frac{\delta W}{W}\right)^2 \right]^{\frac{1}{2}} \qquad (7)$$

$$\frac{\delta f}{f} = \left[\left(\frac{\delta P}{P}\right)^2 + \left(\frac{\delta L}{L}\right)^2 + \left(\frac{\delta Q}{Q}\right)^2 + \left(3\frac{\delta H}{H}\right)^2 + \left(3\frac{\delta W}{W}\right)^2 \right]^{\frac{1}{2}} \qquad (8)$$

The uncertainties in the preceding terms are estimated from manufacturers' specifications and dimensional measurement uncertainties as follows: δQ is $\pm 1.01\%$ of flowmeter reading; δL, δH, and δW are 1 mm, 40 μm, and 5 μm, respectively; and δP is $\pm 0.25\%$ of pressure transducer full scale (138 kPa) including effects of linearity, hysteresis, and repeatability. For a typical measurement, for

example, case L2, $L = 41$ mm, $H = 942$ μm, and $W = 323$ μm, the pressure drop varies from 4.8 to 77.9 kPa as the Reynolds number is increased from 3.79×10^2 to 3.619×10^3 and the estimated uncertainties are

$$\delta Re/Re = 4.6\%, \qquad 5.3\% \leq \delta f/f \leq 8.9\%$$

For all of the cases considered in this study, the uncertainties can be computed in the same manner as described by Eqs. (7) and (8). For the long microchannels, the uncertainties ranged from 4.6 to 10.5% for Reynolds number and from 5.3 to 11.8% for f. Similarly, for the short channels, the corresponding uncertainties ranged from 4.9 to 9.5% for Reynolds number and from 6.2 to 10.9% for f. As indicated by Eqs. (7) and (8), errors in measurement of the microchannel geometry are the greatest contributors to the uncertainty in friction factor. This uncertainty may be one source of discrepancies in the measurements reported in the literature.
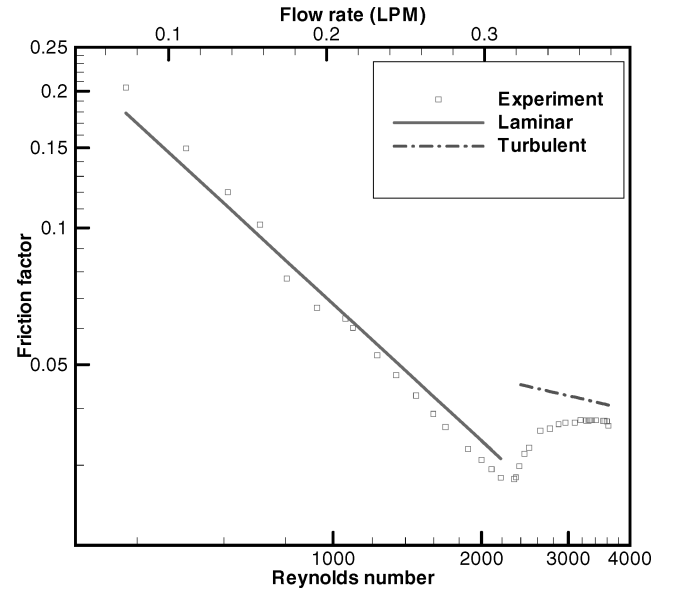
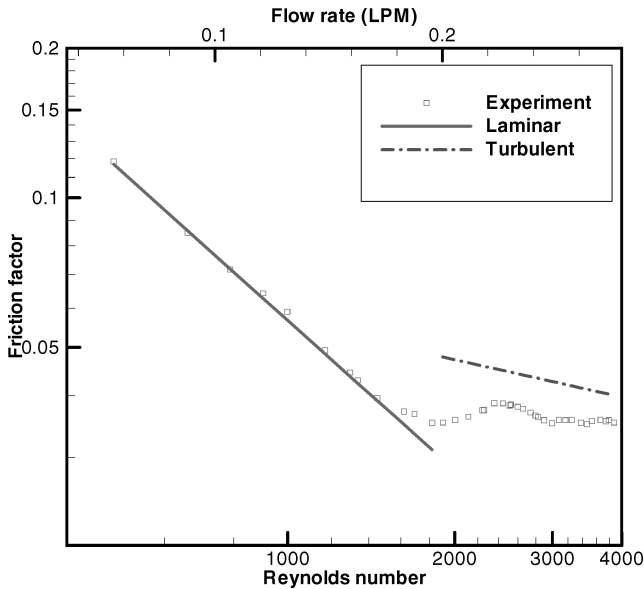## Experimental Results and Discussion

Friction Factors

Experimental results for the long (L series) microchannels are shown in Figs. 3a–3d. The Darcy friction factor is plotted as a
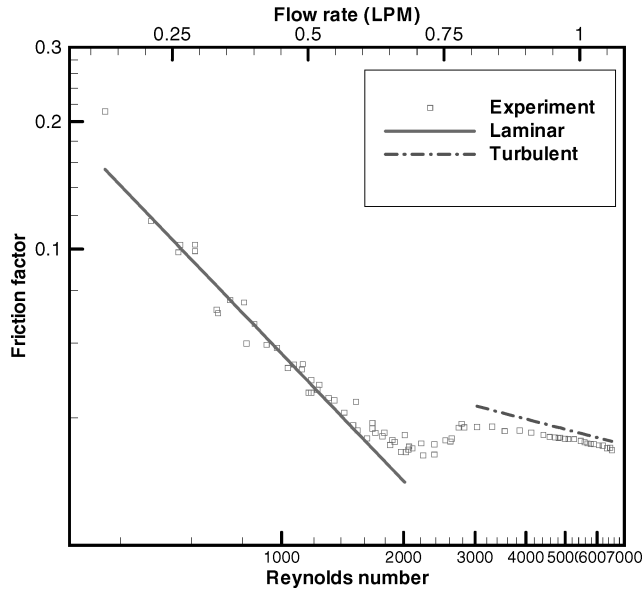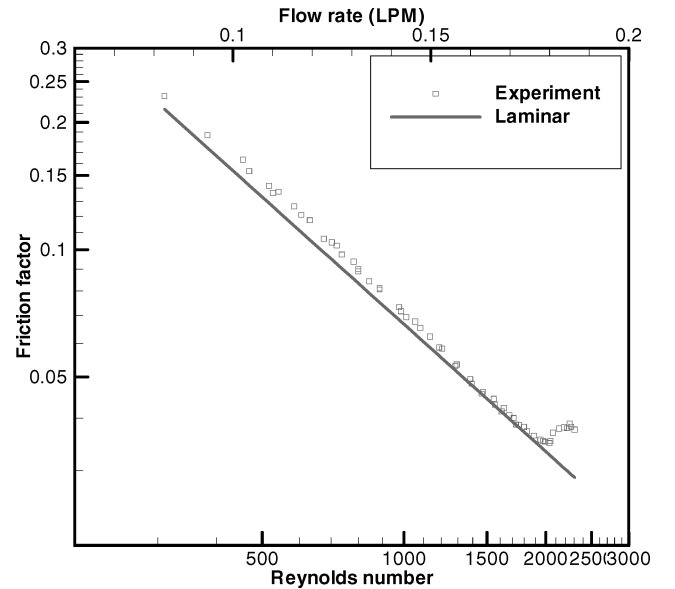

a) L4 ($D_h = 974$ μm)

b) L3 ($D_h = 414$ μm)

c) L2 ($D_h = 481$ μm)

d) L1 ($D_h = 324$ μm)

Fig. 3   Friction factor variation with Reynolds number in long microchannels [laminar predictions from Eq. (3), turbulent from Eq. (4)].

function of Reynolds number. Because the pressure drop in this case does not involve any inlet and exit losses, potential errors in correcting the measurements for losses are avoided. It is seen from Fig. 3 that for all of the cases considered ($324 \leq D_h \leq 974$ μm), the experimental results agree closely with the theoretical predictions in the laminar region. At $Re \approx 2 \times 10^3$, the friction factors from the experiments start to deviate from the laminar predictions, indicating the onset of transition. The onset of transition for the microchannels considered is, thus, seen to agree with the behavior in conventional channels.

Onset of Transition

Transition to turbulence arises essentially from the sensitivity of the flowfield to perturbations such as small changes in initial conditions, boundary conditions, etc. In real flows, no strict theoretical limit exists for the critical Reynolds number at which transition will occur. According to linear instability analysis,[10] the critical Reynolds number for a channel with aspect ratio $\alpha = 8$ should be higher than 1.0261×10^4 and will increase with decreasing aspect ratio. Experimental observations have shown that channel flow can stay laminar for Reynolds numbers up to 5×10^4 if completely undisturbed. With the presence of perturbations, the onset of turbulence will occur for a $Re = 1.8 \times 10^3$ (Ref. 11), below which the flow will remain laminar even with very strong disturbances.

Arguments have been extended in the literature that early transition occurs in microchannels at Reynolds numbers as low as 5×10^2 (Refs. 3 and 4). However recent studies have attributed these low transitional Reynolds numbers to possible experimental errors.[12] Other recent studies have indicated higher transitional Reynolds numbers of approximately 1.5×10^3 (Refs. 11 and 13), which is closer to that observed in conventional channels. Results from the present work also suggest that no such early transition occurs, at least down to hydraulic diameters of approximately 200 μm. Figure 3 also indicates that the transition range extends up to $Re = 4 \times 10^3$ (Figs. 3b and 3c), and there are indications from Fig. 3a that the flow becomes fully turbulent at $Re = 5 \times 10^3$. These values compare favorably to $Re = 3 \times 10^3$, which is considered to be the minimum Reynolds number for fully turbulent flow[14] in conventional channels.

In turbulent flows, Kolmogorov microscales are the smallest scales representing the finest structure in the flow (the smallest feature size at which the kinetic energy is dissipated via viscosity, that is, the smallest eddy). They are related to the rate of dissipation ε due to the fluctuating velocity components and the kinematic viscosity[15] ν

$$\eta = (\nu^3/\varepsilon)^{\frac{1}{4}} \qquad (9)$$

$$\varepsilon = [u(l)]^3/l \qquad (10)$$

It is expected that the smaller the Kolmogorov scales are the more effective the kinetic energy dissipation via molecular viscosity and the more turbulent the flow. In the energy cascade concept,[16] the rate of energy transfer from large scales determines the dissipation rate ε that is at the end of the cascade. Therefore, the Kolmogorov scales can be calculated with information from the mean flowfield, where the large eddies occur. Because any fine structure in the flow would be restricted by the physical dimension of the flow, if the characteristic length scale of the flow were smaller than the Kolmogorov length scale, the flowfield would be dominated by viscous stresses and turbulence would not be sustained.

Taking $u(l)$ as the velocity fluctuation in the mean velocity field, which occurs over the microchannel characteristic dimension l (D_h in this case), the corresponding Kolmogorov length scales for water at 295 K in microchannels of various dimensions are estimated in Table 2.

Several observations can be made from the estimates in Table 2: 1) For fixed microchannel size, reduced fluctuations in the mean velocity field will result in a larger Kolmogorov length scale, as well as smaller dissipation rate. Thus, the flow would tend to be more stable. 2) For fixed velocity fluctuations, decreasing the microchannel dimension will result in a larger value of η/l because $\eta/l \propto l^{-3/4}$. When this ratio exceeds unity, turbulent structures may

Table 2   Estimation of Kolmogorov length scale[a]

Velocity fluctuation $u(l)$, m/s	Channel size l, m	Dissipation rate ε, m^2/s^3	Kolmogorov length scale η, m	η/l
1	0.1	10	0.0031	0.03
0.1	0.1	0.01	0.0172	0.17
1	0.01	1×10^2	0.00172	0.17
0.1	0.01	0.1	0.0097	0.97
1	0.001	1×10^3	0.00097	0.97
0.1	0.001	1	0.0055	5.50
1	0.0001	1×10^4	0.00055	5.50
0.1	0.0001	10	0.0031	31.00
10	0.0001	1×10^7	0.000097	0.97

[a]Kinematic viscosity $\nu = 0.00096$ m^2/s.

not be sustained in the small physical dimensions available, thus, preventing the flow from becoming fully turbulent. 3) For fixed velocity fluctuations, the impact of microchannel size on the turbulent flow becomes pronounced only when the channel size is sufficiently small. For instance, when $u(l) = 1$ m/s, l needs to be on the order of 1 mm before $\eta/l \approx 1$. The effect becomes less pronounced for larger dimensions, but is more apparent for reduced dimensions. This may help explain the trends in Fig. 3: Because all of the microchannel hydraulic diameters considered are less than 1 mm, even for an aggressive estimate for velocity fluctuation $u(l)$ of 1 m/s, the Kolmogorov length scale will be larger than the microchannel dimension D_h, which makes fully turbulent flow less likely. As a result, the experimental data fail to match the theoretical predictions in the Reynolds number range of $3 \times 10^3 \sim 4 \times 10^3$, which assume fully developed turbulence. 4) For a microchannel of 0.1-mm dimension, only when $u(l)$ reaches 10 m/s is the Kolmogorov length scale small enough to become comparable to the microchannel dimension at which fully developed turbulent flow can be sustained. This implies that, for very small microchannel dimensions, it is very difficult to sustain fully developed turbulent flows. 5) The information on velocity fluctuations is crucial in the preceding estimates. This suggests the need for obtaining more detailed information in future research into turbulent microchannel transport.

Friction Factors with Pressure Losses

Experiments were also performed in short (S series) microchannels to examine the validity of correcting for inlet and exit losses using conventional correlations (as described in the Appendix). Results for these short microchannels are shown in Figs. 4a–4e. The symbols in Fig. 4 indicate measured pressure drops that have been corrected as per Eq. (6). The good agreement between experiment and conventional correlations in the laminar regime validates the methodology for correction of inlet and exit losses. In the turbulent regime, on the other hand, satisfactory correlations for the losses are not readily available.

Flow Visualization

To verify the onset of transition to turbulence, flow visualization was performed using a dye entrained into the flow upstream of the microchannels. The pressure port was used as the dye well from which a steady stream of potassium permanganate solution was released into the flow. Because the dye is a dilute aqueous solution, it can be considered to be neutrally buoyant. The images were collected using a color video system consisting of a $6\times$–$300\times$ video inspection microscope and a charge-coupled device camera. The observations were made near the midpoint along the length of the microchannel.

In the flow visualization, onset of transition is considered to occur when the dye streaks entrained into the flow start to diffuse and blur. The measured flow rate allows a determination of the corresponding Reynolds number. Results for flow visualization in microchannels with hydraulic diameters of 271 and 470 μm are shown in Figs. 5 and 6. The flow is from left to right.

Figure 5 shows the flow behavior at different Reynolds numbers in microchannel S2, $D_h = 271$ μm. At low Reynolds numbers

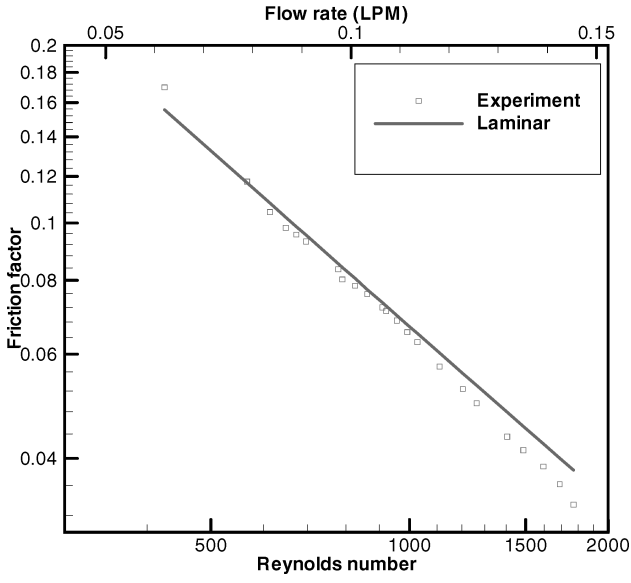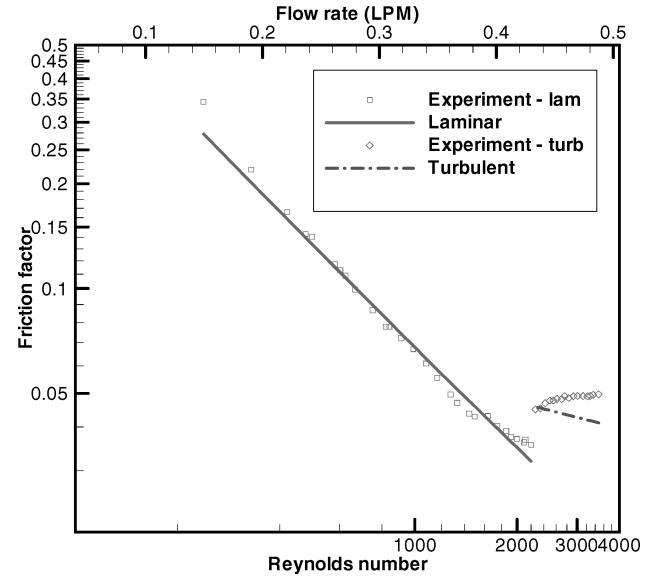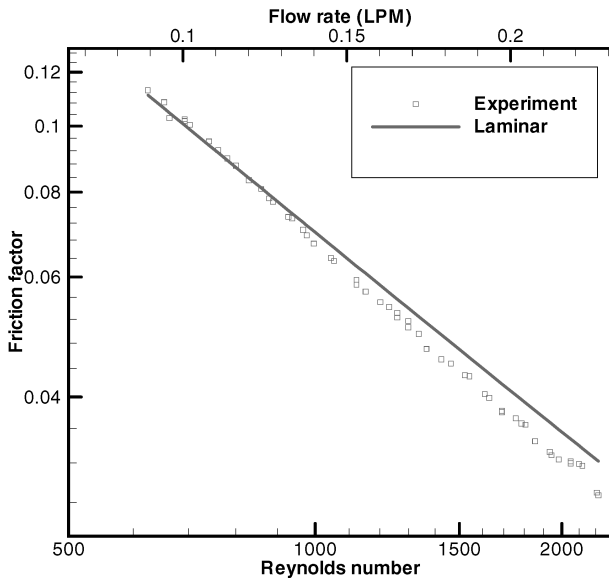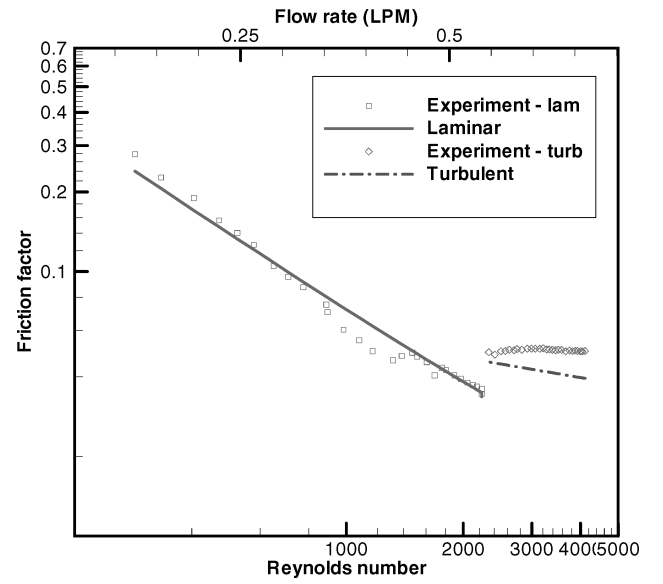a) S1 ($D_h = 244\ \mu$m)

b) S2 ($D_h = 271\ \mu$m)

c) S3 ($D_h = 410\ \mu$m)

d) S4 ($D_h = 459\ \mu$m)
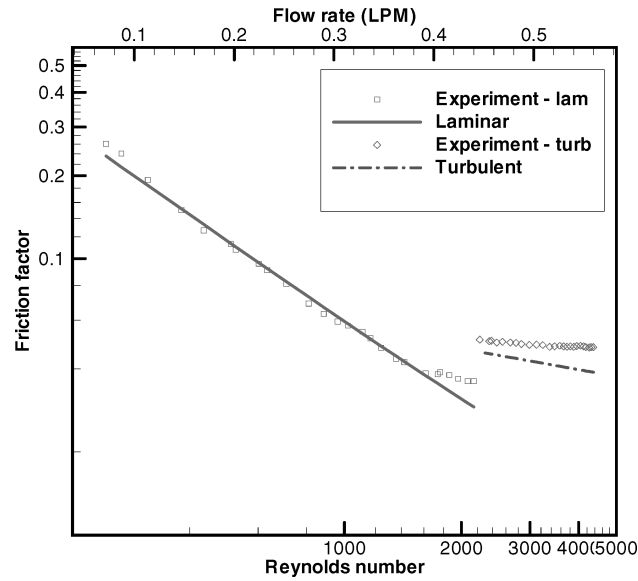
e) S5 ($D_h = 470\ \mu$m)

Fig. 4 Corrected friction factor variation with Reynolds number in short microchannels [laminar predictions from Eq. (5), turbulent from Eq. (4)].
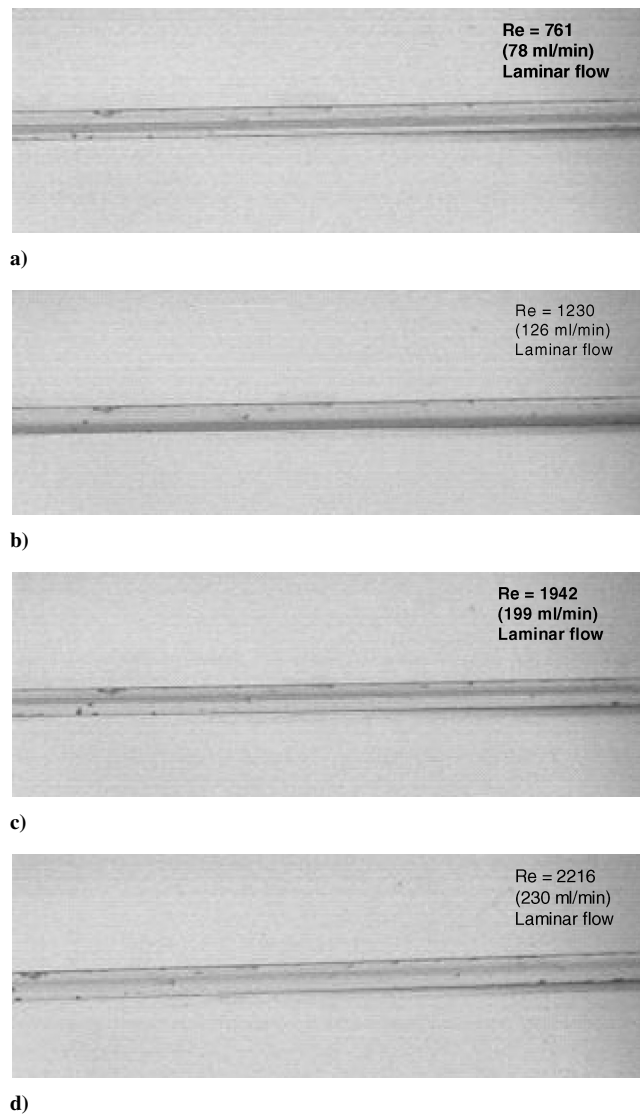
Fig. 5 Flow visualization in a short microchannel, S2: $W = 180\ \mu$m and $D_h = 271\ \mu$m.

($Re = 7.61 \times 10^2$ and 1.23×10^3), there is virtually no diffusion of the dye streaks all along the channel, and the streakline remains clearly demarcated. At $Re = 1.942 \times 10^3$, although the dye streak is less distinct, this is a result of reduced dye density caused by the higher flow velocity and not due to turbulent diffusion. Even at $Re = 2.216 \times 10^3$, the dye streaks can still be recognized, suggesting that the flow remains laminar in this entire Reynolds number range, as suggested also by the results in Fig. 4b.

Flow visualization results for a larger microchannel (S5, $W = 480\ \mu$m) are shown in Fig. 6. The reduced liquid velocity for a given Reynolds number in this case, coupled with a larger field of view, allows a better resolution. At low Reynolds numbers ($Re = 5.88 \times 10^2$ and 1.078×10^3), there is no diffusion of the dye streaks all along the microchannel, and the straight streakline has sharp edges. At $Re = 1.802 \times 10^3$, the edge of the dye streak starts to blur, indicating the onset of transition. By $Re = 2.202 \times 10^3$, the dye is almost completely diffused. Transition to turbulence in this case may be considered to have occurred at a Reynolds number of approximately 1.8×10^3. These visualizations again agree with the observations from the measured pressure drops, which showed that the flow can stay laminar up to $Re \approx 2 \times 10^3$.

Numerical Analysis

Computations of microchannel flow and heat transfer that include a consideration of the inlet/outlet sections are needed for any realistic microchannel heat sink implementation. The present simu-
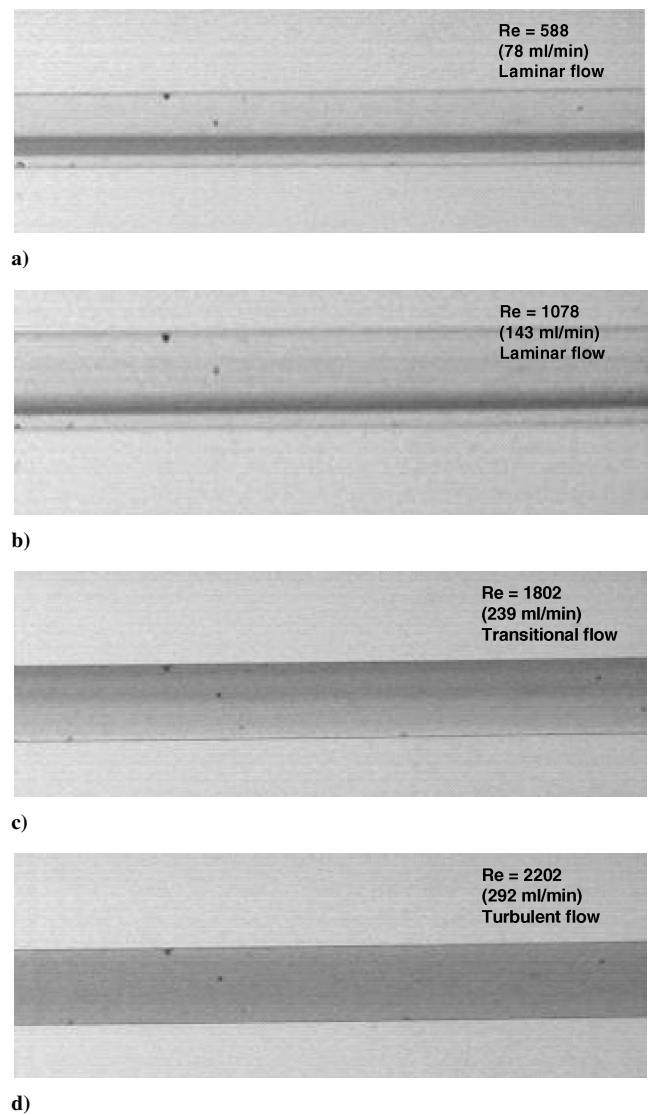

Fig. 6 Flow visualization in a wider microchannel, S5: $W = 480\ \mu$m and $D_h = 470\ \mu$m.
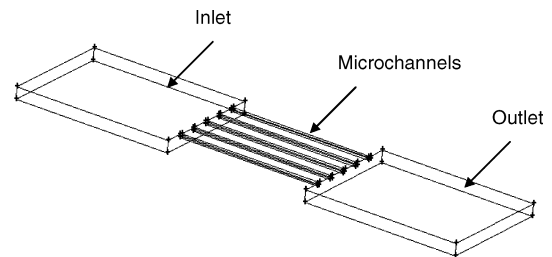

Fig. 7 Computational domain for flow calculations in the microchannel test section.

lations were targeted at evaluating the overall pressure drop in such a simulation.

A general-purpose finite volume-based computational fluid dynamics (CFD) software package (FLUENT[17]) was used for these computations. The working fluid, which is water in this case, was considered to be incompressible, and its properties were assumed constant. Only flow rates in the laminar regime were considered. The calculation domain is shown in Fig. 7. Results for simulations in the microchannel test section S5 ($W = 480\ \mu$m and $H = 460\ \mu$m) are presented here. The grid consists of 270,000 computational cells. A mesh of hexahedral elements was employed with the Cooper scheme.
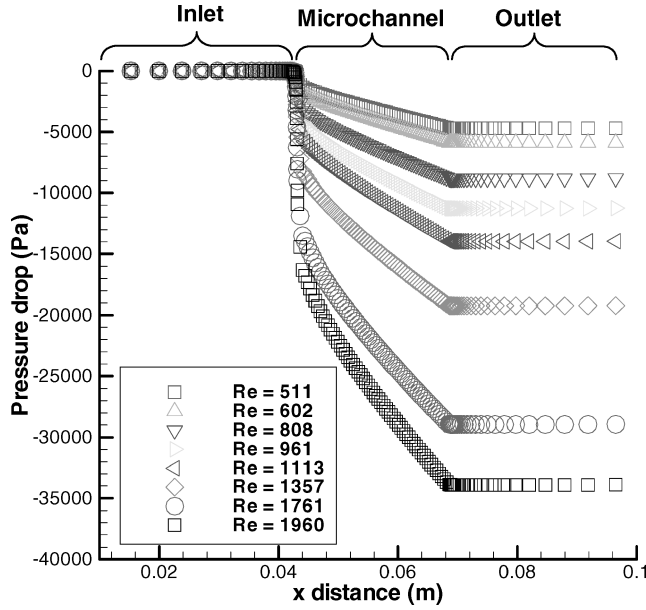
Fig. 8 Pressure drop for different Reynolds numbers, S5:
$D_h = 470 \ \mu$m.

To resolve the flow field accurately in critical regions such as within the microchannels and at the inlet/outlet interfaces, the mesh was locally refined. The inlet velocity was specified and an out-flow condition assigned at the outlet. The convective terms were discretized using a first-order upwind scheme for all equations. A computational grid of $15 \times 15 \times 60$ cells was used within the microchannel. Simulations with different grids showed a satisfactory grid independence for the results obtained with this mesh. For the case of $Re = 1.113 \times 10^3$, for instance, with the same inlet conditions the pressure drop along the microchannel was 7.83 kPa for the $15 \times 15 \times 60$ mesh in the microchannel and 7.99 kPa for a coarser mesh ($10 \times 10 \times 50$).

The liquid is driven through the inlet and is accelerated at the abrupt contraction into the microchannels. Either the pressure drop within the microchannel or the entrance loss dominates the overall pressure drop, depending on the flow rate. This trend is clearly indicated in Fig. 8, which shows that the pressure drop increases significantly at the higher flow rates. A closer examination of the results in Fig. 8 reveals several interesting features: 1) The significant flow contraction at the entrance to the microchannel causes a sharp drop in the pressure. 2) It is clear that the inlet pressure losses account for quite a large fraction of the overall pressure drop at the higher flow rates, pointing to the importance of a careful consideration of these losses in microchannel heat sink design. 3) The length required for the pressure drop per unit length to reach a constant value may be determined as

$$x/D_h = C \, Re \tag{11}$$

where C is a constant depending on the geometry (0.033, 0.046, and 0.057 for aspect ratios of 10, 5, and 1, respectively[18]). It can be seen in Fig. 9 that, at low Reynolds numbers, the flow becomes fully developed some distance into the microchannel, for example, at $Re = 5.11 \times 10^2$, the pressure gradient is nearly constant from $x = 0.055$ m, signifying an entrance length of 0.012 m. [This compares to a value of x predicted from Eq. (11) of 0.011 m.] In contrast, at higher Reynolds numbers, the flow continues to develop throughout the length of the microchannel, for example, at $Re = 1.113 \times 10^3$, the entrance length is 0.024 m, which covers virtually the entire length of the microchannel, $L = 0.025$ m. Consequently, the apparent friction factor, as in Eq. (5), should be employed in interpreting the experimental data in such developing flow in microchannels.

A comparison of the numerically predicted overall pressure drop in the microchannels against the experimentally determined values

Table 3   Measured and predicted overall pressure drops in the S5 microchannels

$Re \times 10^2$	ΔP numerical, Pa	ΔP experimental, Pa	Difference, %
5.11	5,012	5,523	9
6.02	6,254	6,765	8
8.08	9,119	9,665	6
9.60	11,358	12,288	8
11.13	13,953	15,463	10
13.57	18,011	20,158	11
17.61	29,114	31,203	9
19.60	33,021	37,279	11

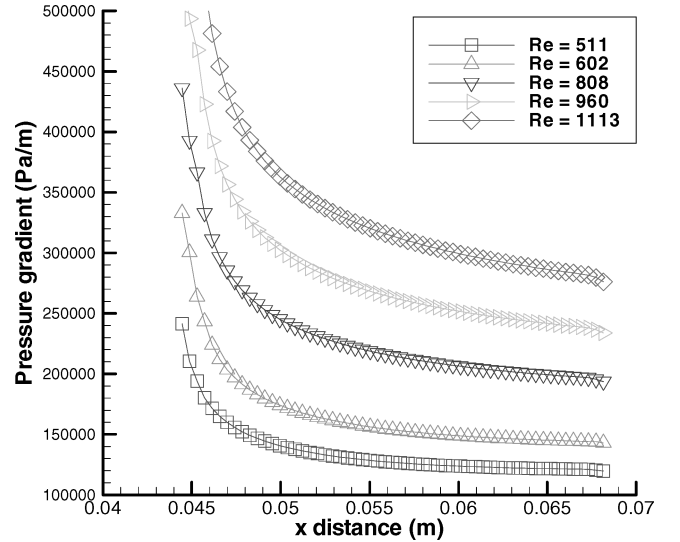**Fig. 9   Pressure gradient in the microchannel for different Reynolds numbers, S5:** $D_h = 470 \ \mu$m.

is shown in Table 3. The two sets of results are seen to show satisfactory agreement, considering the complexity of the system-level flowfield, which suggests that a conventional CFD analysis approach can be employed in predicting flow behavior in the microchannels considered in this study.

Conclusions

Experimental measurements and numerical simulations have been performed, along with flow visualization and analysis, to study the behavior of liquid flow in microchannels. It is found that conventional theory offers reliable predictions for the flow characteristics in microchannels up to a Reynolds number of approximately 2×10^3, in the range of hydraulic diameters considered (244–974 μm). There is also support for the argument that the development of fully turbulent flow is retarded in microchannels. The estimated Kolmogorov length scales suggest that the reduced microchannel size may have a significant impact on the development of turbulence. The onset of transition to turbulence in microchannels was qualitatively corroborated by flow visualization. The fact that the results of numerical simulations were in satisfactory agreement with the experimental measurements indicates that commercial software packages can be employed to aid the study of flow characteristics in microchannels.

Appendix: Pressure Loss Correction

The construction of a microchannel heat sink usually involves contraction and expansion at the entrance and exit of the microchannels. These abrupt flow area changes introduce additional local pressure drops. The overall pressure loss through the microchannel system consists of three parts,[19]

$$\Delta P = (P_1 - P_2) + (P_2 - P_3) + (P_3 - P_4) \tag{A1}$$

in which $(P_2 - P_3)$ is the pressure drop in the microchannel, $(P_1 - P_2)$ is the contraction pressure loss, and $(P_3 - P_4)$ is the
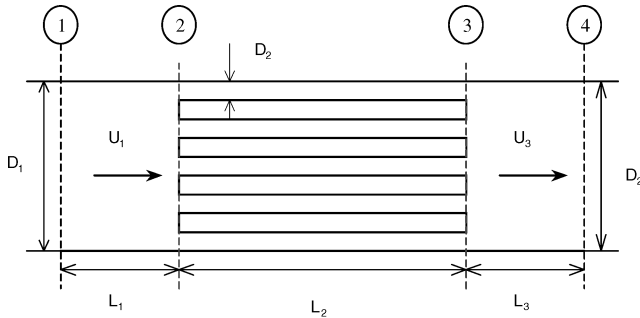
Fig. A1 Microchannel test section (including inlet, microchannel, and outlet sections) where A indicates the areas and positions 1 and 4 are the locations of pressure taps: a) top view and b) side view.
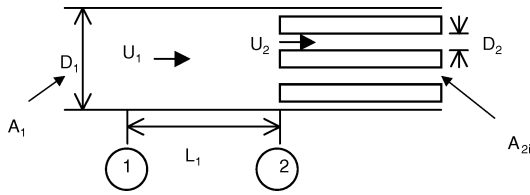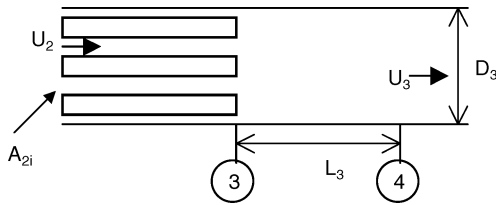

Fig. A2 Entrance contraction.

Fig. A3 Exit expansion.

expansion pressure loss. Figure A1 shows the locations of pressures 1–4.

The pressure loss due to flow contraction at the entrance (Fig. A2) is given by

$$P_1 - P_2 = \left[1 - (A_2/A_1)^2 + K_1\right]\tfrac{1}{2}\rho U_2^2 + (f_1 L_1/D_1)\tfrac{1}{2}\rho U_1^2 \quad (A2)$$

where A_1 is the inlet cross-sectional area and

$$A_2 = \sum_i A_{2i}$$

is equal to the sum of flow areas. For laminar flow, the nonrecoverable loss coefficient is given by

$$K_1 = 0.0088\alpha^2 - 0.1785\alpha + 1.6027 \quad (A3)$$

Because the inlet section is usually too short for the flow to become fully developed, fRe should be evaluated from Eq. (5). For turbulent flow, the nonrecoverable loss coefficient is given by

$$K_1 = \tfrac{1}{2}(1 - A_2/A_1) \quad (A4)$$

The pressure loss due to flow expansion at the exit (Fig. A3) has to be considered separately for laminar and turbulent flows because of the nonuniform flow profile at the exit. For laminar flow, the exit pressure loss is given by

$$(P_3 - P_4)\Big/\tfrac{1}{2}\rho U_2^2 = -2\beta(A_2/A_3)(1 - A_2/A_3) + f_3 L_3/D_3 \quad (A5)$$

where A_3 is the outlet cross-sectional area,

$$A_2 = \sum_i A_{2i}$$

is equal to sum of flow areas, and the flow profile factor $\beta = 1.33$. For turbulent flow, the pressure loss is estimated by

$$(P_3 - P_4)\Big/\tfrac{1}{2}\rho U_2^2 = (A_2/A_3)^2 - 1 + K_3 + f_3 L_3/D_3 \quad (A6)$$

where the nonrecoverable loss coefficient is

$$K_3 = [1 - (A_2/A_3)]^2 \quad (A7)$$

Acknowledgment

References

[1]Peng, X. F., Peterson, G. P., and Wang, B. X., "Frictional Flow Characteristics of Water Flowing Through Microchannels," *Experimental Heat Transfer*, Vol. 7, No. 4, 1994, pp. 265–283.

[2]Yu, D., Warrington, R., Barron, R., and Ameel, T., "An Experimental and Theoretical Investigation of Fluid Flow and Heat Transfer in Microtubes," *ASME/JSME Thermal Engineering Conference*, Vol. 1, American Society of Mechanical Engineers, Fairfield, NJ, 1995, pp. 523–530.

[3]Mala, G. M., and Li, M., "Flow Characteristics of Water in Microtubes," *International Journal of Heat and Fluid Flow*, Vol. 20, No. 2, 1999, pp. 142–148.

[4]Mala, G. M., Li, D., and Dale, J. D., "Heat Transfer and Fluid Flow in Microchannels," *International Journal of Heat Mass Transfer*, Vol. 40, No. 13, 1997, pp. 3079–3088.

[5]Sobhan, C. B., and Garimella, S. V., "A Comparative Analysis of Studies on Heat Transfer and Fluid Flow in Microchannels," *Microscale Thermophysical Engineering*, Vol. 5, No. 4, 2001, pp. 293–311.

[6]Garimella, S. V., and Sobhan, C. B., "Transport in Microchannels—A Critical Review," *Annual Review of Heat Transfer*, Vol. 13, 2003 (in press).

[7]Xu, B., Ooi, K. T., Wong, N. T., and Choi, W. K., "Experimental Investigation of Flow Friction for Liquid Flow in Microchannels," *International Communications in Heat and Mass Transfer*, Vol. 27, No. 8, 2000, pp. 1165–1176.

[8]Shah, R. K., and London, A. L., "Laminar Flow Forced Convection in Ducts," *Advances in Heat Transfer*, Supplement 1, Academic Press, 1978.

[9]Figliola, R. S., and Beasley, D. E., *Theory and Design for Mechanical Measurements*, Wiley, New York, 2000.

[10]Tatsumi, T., and Yoshimura, T., "Stability of the Laminar Flow in a Rectangular Duct," *Journal of Fluid Mechanics*, Vol. 212, 1990, pp. 437–449.

[11]Sharp, K. V., Adrian, R. J., and Beebe, D. J., "Anomalous Transition to Turbulence in Microtubes," *Proceedings of the 2000 ASME International Mechanical Engineering Congress and Exposition*, MEMS, Vol. 2, American Society of Mechanical Engineers, Fairfield, NJ, 2000, pp. 461–466.

[12]Obot, N. T., "Toward a Better Understanding of Friction and Heat/Mass Transfer in Microchannels—A Literature Review," *Heat Transfer and Transport Phenomena in Microsystems*, Begell House, New York, 2000, pp. 72–80.

[13]Harms, T. M., Kazmierczak, M. J., and Gerner, F. M., "Experimental Investigation of Heat Transfer and Pressure Drop Through Deep Microchannels in a (110) Silicon Substrate," *Proceedings of the ASME Heat Transfer Division*, Vol. 1, American Society of Mechanical Engineers, Fairfield, NJ, 1997, pp. 347–357.

[14]Patel, V. C., and Head, M. R., "Some Observations on Skin Friction and Velocity Profiles in Fully Developed Pipe and Channel Flows," *Journal of Fluid Mechanics*, Vol. 38, 1969, pp. 181–201.

[15]Tennekes, H., and Lumley, J. I., *A First Course in Turbulence*, MIT Press, Cambridge, MA, 1972.

[16]Pope, S. B., *Turbulent Flows*, Cambridge Univ. Press, Cambridge, England, U.K., 2000.

[17]"Fluent User's Guide," Fluent Inc., Lebanon, NH, 1998.

[18]Hartnett, J. P., Koh, J. C. Y., and McComas, S. T., "A Comparison of Predicted and Measured Friction Factors for Turbulent Flow Through Rectangular Ducts," *Journal of Heat Transfer*, Vol. 84, No. 1, 1962, pp. 82–88.

[19]Blevins, R. D., *Applied Fluid Dynamics Handbook*, Krieger, Malabar, FL, 1992, pp. 77–78.